Ferrofilm in a magnetic field

Randy Back[1,*] and J. Regan Beckham[2,†]

[1]*Department of Chemistry, The University of Texas at Tyler, 3900 University Blvd., Tyler, TX 75799, USA*
[2]*Department of Mathematics, The University of Texas at Tyler, 3900 University Blvd., Tyler, TX 75799, USA*

A vertically draining thin ferrofilm under the influence of gravity and a nonuniform magnetic field is considered. It is observed experimentally that the presence of the magnetic field greatly alters the drainage of the film. A mathematical model is developed to describe the behavior. Experiments are conducted for multiple magnetic field configurations. The model is solved for two different sets of boundary conditions and results are compared to experiments. It is shown that the magnetic field structure, the concentration of magnetite in the solution, and the boundary conditions all have noticeable affects on the evolution of the thinning film. Good qualitative agreement between the model and the experiments is observed.

PACS number(s): 47.15.−x, 75.70.−i

I. INTRODUCTION

The scientific study of thin films can be traced all the way back to da Vinci with the study of soap bubbles. Thin film behavior caught the interest of prominent scientists such as Plateau, Newton, Laplace, Gauss, and Poisson. Their interest stems from their appearance in biological and engineered systems alike. One particular area of interest is the draining and thinning of soap films. Much of the early work was done by Plateau and Gibbs, and this study was continued by Mysels *et al.* [1]. The draining film is still of interest today and new models are still being proposed to describe its behavior [2]. We make no attempt to give an exhaustive history of the field. For the interested reader, see Ref. [3] and references therein. In addition to the draining thin film aspect of our problem, we must consider the ferrohydrodynamic nature of our problem. The field of ferrohydrodynamics was developed in the early 1960s [4] and, like the study of thin films, is still developing today. For information about the development of the field we refer the reader to Ref. [5]. From the interest in pattern formation [6] to fluid control used in drug delivery [7] and more recently the use of ferrofluid films in sensing [8], it is clear that the ability to describe a ferrofilm is necessary to fully realize the potential of devices that employ these structures. The effects of magnetic fields on thin films is also an important area of study in the development of micromechanical devices [9]. In our current problem we explore the vertical drainage of a ferrofilm in the presence of a nonuniform magnetic field. In our experiments bar magnets are used to generate the magnetic field. This topic was initially explored experimentally by Elias *et al.* [10]. An early mathematical model and its analysis were done by Moulton *et al.* in Refs. [11,12].

In Ref. [12] the authors develop a model to describe reverse drainage of a ferrofilm due to a magnetic field. There are two main topics that we wish to expand upon. First is the model itself. In Ref. [12] the magnet is modeled as a large circular loop so that the magnetic field only has a vertical component and the resulting model does not include the transverse direction. We develop a model that includes this transverse direction and likewise we consider magnetic fields that

have significant vertical and horizontal components. Second we expand the experimental results. We perform experiments for multiple magnetic field configurations and compare with the solutions obtained from the model. The experimental results in Ref. [12] show thinning regions due to reverse drainage, but there is no formation of a black film region. This is mainly due to the soap solution used and the drainage time, which is ∼ 30 s. In our experiments the film drains until there is a significant black film region. This allows us to better compare the structure of the film to the model simulations. We consider the effects of both magnetite particle concentration in the thin film solution as well as the magnetic field structure. Through these extensions we hope to gain a better understanding of how magnetic fields affect thin ferrofluid films.

The paper is organized as follows. In Sec. II we derive the mathematical model for the system under consideration. Then, in Sec. III we explore the physical problem experimentally and the mathematical model numerically. We conclude in Sec. IV with a summary of our findings along with a discussion of the challenges we faced and possible areas to explore in the future.

II. MATHEMATICAL MODEL

Here we construct a mathematical model for the behavior of a vertically draining thin film under the influences of surface tension, gravity, and an external magnetic field. Our desire is to arrive at a differential equation that will describe the free surface of the film and will thus describe the thickness within the film (see Fig. 1). Letting $\mathbf{u}' = (u',v',w')$, the Navier-Stokes equations require that $\mathbf{u}'$ satisfy

$$\mathbf{\nabla} \cdot \mathbf{u}' = 0, \tag{1}$$

$$\rho\left(\frac{\partial \mathbf{u}'}{\partial t} + \mathbf{u}' \cdot \mathbf{\nabla}\mathbf{u}'\right) = \mu\nabla^2\mathbf{u}' - \mathbf{\nabla}p' + \rho g\hat{\mathbf{x}} + \mathbf{BF}'. \tag{2}$$

Equation (1) is the requirement that the fluid is incompressible. Equation (2) is the force balance equation, where ρ is the fluid density, p' is the pressure, g is the gravitational constant, μ is the dynamic viscosity, and $\mathbf{BF}'$ is the body force acting on the film due to the magnetic field. From Ref. [5], assuming that the solution is a dilute colloidal solution of magnetic particles, we have that the body force due to a magnetic field is

$$\mathbf{BF}' = \mu_0(\mathbf{M} \cdot \mathbf{\nabla})\mathbf{H}',$$

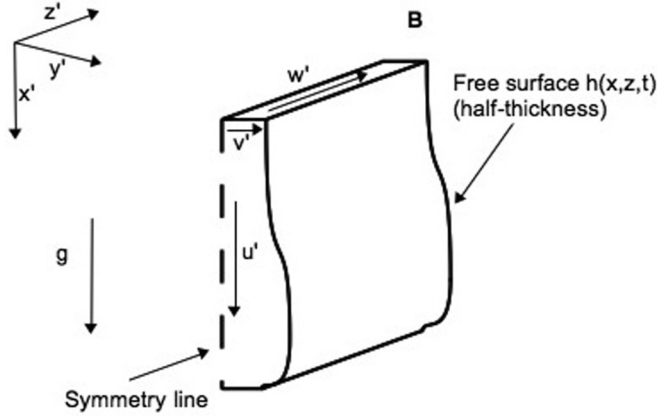*rback@uttyler.edu
†Corresponding author: rbeckham@uttyler.edu

FIG. 1. Thin ferrofilm under the influence of gravity g and magnetic field **B**.

where μ_0 is the magnetic permeability of free space. Since the ferrofluid is paramagnetic, the magnetization $\mathbf{M}'$ is aligned with the applied field $\mathbf{H}'$ and further assuming a linear media gives $\mathbf{M}' = \chi_m \mathbf{H}'$, where χ_m is the susceptibility constant [13]. Given these assumptions we have

$$
\begin{aligned}
\mathbf{BF}' &= \mu_0 \chi_m (\mathbf{H}' \cdot \nabla)\mathbf{H}' \\
&= \mu_0 \chi_m (H_1' H_{1x}' + H_2' H_{1y}' + H_3' H_{1z}', H_1' H_{2x}' + H_2' H_{2y}' \\
&\quad + H_3' H_{2z}', H_1' H_{3x}' + H_2' H_{3y}' + H_3' H_{3z}') \\
&= \mu_0 \chi_m (BF'^{(x)}, BF'^{(y)}, BF'^{(z)}).
\end{aligned}
$$

We shall make the assumption that the film is symmetric about the centerline $y' = 0$ so that $\frac{\partial u'}{\partial y'} = 0$, $\frac{\partial w'}{\partial y'} = 0$, and $v' = 0$. At the free surface of the film $y' = h'(x', z', t')$, we impose the following three conditions.

(i) The kinematic condition states that fluid that starts on the boundary remains on the boundary:

$$
\frac{\partial h'}{\partial t'} = v' - u' \frac{\partial h'}{\partial x'} - w' \frac{\partial h'}{\partial z'}. \tag{3}
$$

(ii) The normal stress balance gives that the change in momentum across the interface is balanced by the surface tension of the interface:

$$
[\hat{n} \cdot T \cdot \hat{n}] = \gamma \bar{H}. \tag{4}
$$

Here $\hat{n}$ is the unit normal, T is the stress tensor, γ is the surface tension, and $\bar{H}$ is the mean curvature.

(iii) Tangential immobility requires that tangential velocity components of the fluid at the surface must vanish:

$$
u' = 0, \quad w' = 0. \tag{5}
$$

As noted in Ref. [12], this condition is not necessary in general, but can be assumed based on the solution recipe.

The conditions at the boundary of the frame are that of a fixed thickness of the film, equal to the frame thickness, and that there is no flux through the frame. The formulation of these conditions will be suppressed until later in the derivation, at which time it will be apparent. At this stage we nondimensionalize with a proper scaling of the dependent

and independent variables as follows:

$$
x = \frac{x'}{L}, \quad y = \frac{y'}{h_0}, \quad z = \frac{z'}{L}, \quad u = \frac{u'}{U_0}, \quad v = \frac{v'}{\epsilon U_0},
$$

$$
w = \frac{w'}{U_0}, \quad t = \frac{U_0 t'}{L}, \quad p = \frac{h_0^2 p'}{\mu L U_0}.
$$

Here $L = (\gamma/\rho g)^{1/2}$ is a balance of the surface tension and gravity, h_0 is a characteristic length scale for the film thickness, and $U_0 = \rho g h_0^2 / \mu$ is our vertical and transversal velocity scaling. Since we have a thin film, L ($\backsim 2$ mm) is large compared to h_0 ($\backsim 10$ μm). For this reason we define $\epsilon = h_0/L$, which is a small parameter $[O(10^{-3})]$. For the magnetic field, we scale by a characteristic value for the applied field H_0'. Since the film is thin we will assume that there will be no y dependence to leading order. Nondimensionalizing Eqs. (1) and (2) gives

$$
\frac{U_0}{L}\left(\frac{\partial u}{\partial x} + \frac{\partial v}{\partial y} + \frac{\partial w}{\partial z}\right) = 0,
$$

$$
\rho \frac{\epsilon U_0^2}{h_0}\left(\frac{\partial u}{\partial t} + u\frac{\partial u}{\partial x} + v\frac{\partial u}{\partial y} + w\frac{\partial u}{\partial z}\right)
$$
$$
= \mu\left(\frac{\epsilon^2 U_0}{h_0^2}\frac{\partial^2 u}{\partial x^2} + \frac{U_0}{h_0^2}\frac{\partial^2 u}{\partial y^2} + \frac{\epsilon^2 U_0}{h_0^2}\frac{\partial^2 u}{\partial z^2}\right)
$$
$$
- \mu \frac{U_0}{h_0^2}\frac{\partial p}{\partial x} + \rho g + \frac{\mu_0 \chi_m H_0'^2}{L} BF^{(x)},
$$

$$
\rho \frac{\epsilon^2 U_0^2}{h_0}\left(\frac{\partial v}{\partial t} + u\frac{\partial v}{\partial x} + v\frac{\partial v}{\partial y} + w\frac{\partial v}{\partial z}\right)
$$
$$
= \mu\left(\frac{\epsilon^3 U_0}{h_0^2}\frac{\partial^2 v}{\partial x^2} + \frac{\epsilon U_0}{h_0^2}\frac{\partial^2 v}{\partial y^2} + \frac{\epsilon^3 U_0}{h_0^2}\frac{\partial^2 v}{\partial z^2}\right) - \mu \frac{U_0}{h_0^2}\frac{\partial p}{\partial y},
$$

$$
\rho \frac{\epsilon U_0^2}{h}\left(\frac{\partial w}{\partial t} + u\frac{\partial w}{\partial x} + v\frac{\partial w}{\partial y} + w\frac{\partial w}{\partial z}\right)
$$
$$
= \mu\left(\frac{\epsilon^2 U_0}{h_0^2}\frac{\partial^2 w}{\partial x^2} + \frac{U_0}{h_0^2}\frac{\partial^2 w}{\partial y^2} + \frac{\epsilon^2 U_0}{h_0^2}\frac{\partial^2 w}{\partial z^2}\right)
$$
$$
- \mu \frac{U_0}{h_0^2}\frac{\partial p}{\partial z} + \frac{\mu_0 \chi_m H_0'^2}{L} BF^{(z)}.
$$

Assuming ϵ to be a small parameter, we simplify our model. To leading order we have

$$
\frac{\partial u}{\partial x} + \frac{\partial v}{\partial y} + \frac{\partial w}{\partial z} = 0, \tag{6}
$$

$$
\frac{\partial^2 u}{\partial y^2} - \frac{\partial p}{\partial x} + 1 + \lambda BF^{(x)} = 0, \tag{7}
$$

$$
-\frac{\partial p}{\partial y} = 0, \tag{8}
$$

$$
\frac{\partial^2 w}{\partial y^2} - \frac{\partial p}{\partial z} + \lambda BF^{(z)} = 0, \tag{9}
$$

where $\lambda = \frac{\mu_0 \chi_m H_0'^2}{\rho g L}$. Now we recast our boundary conditions. At $y = 0$ we have

$$
\frac{\partial u}{\partial y} = 0, \quad \frac{\partial w}{\partial y} = 0, \quad v = 0
$$

and at the free surface, $y = h(x,z,t)$ we have

$$u = 0, \quad \frac{\partial h}{\partial t} = v - u\frac{\partial h}{\partial x} - w\frac{\partial h}{\partial z}.$$

Using the incompressibility equation, along with the boundary conditions at $y = h(x,z,t)$, gives

$$\frac{\partial h}{\partial t} = v - u\frac{\partial h}{\partial x} - w\frac{\partial h}{\partial z} = v$$

$$= -\int_0^h \left(\frac{\partial u}{\partial x} + \frac{\partial w}{\partial z}\right) dy \quad (u_x + v_y + w_z = 0).$$

Since $p_y = 0$, we can easily integrate to get u and w. Doing this gives

$$u = \left(\frac{\partial p}{\partial x} - 1 - \lambda B F^{(x)}\right)\left(\frac{y^2}{2} - \frac{h^2}{2}\right)$$

and

$$w = \left(\frac{\partial p}{\partial z} - \lambda B F^{(z)}\right)\left(\frac{y^2}{2} - \frac{h^2}{2}\right).$$

Upon substitution into our kinematic condition we get

$$\frac{\partial h}{\partial t} = -\frac{\partial}{\partial x}\int_0^h u\,dy - \frac{\partial}{\partial z}\int_0^h w\,dy$$

$$= \frac{\partial}{\partial x}\left[\frac{h^3}{3}\left(\frac{\partial p}{\partial x} - 1 - \lambda B F^{(x)}\right)\right]$$

$$+ \frac{\partial}{\partial z}\left[\frac{h^3}{3}\left(\frac{\partial p}{\partial z} - \lambda B F^{(z)}\right)\right].$$

At this point we have

$$\frac{\partial h}{\partial t} - \frac{\partial}{\partial x}\left[\frac{h^3}{3}\left(\frac{\partial p}{\partial x} - 1 - \lambda B F^{(x)}\right)\right]$$

$$- \frac{\partial}{\partial z}\left[\frac{h^3}{3}\left(\frac{\partial p}{\partial z} - \lambda B F^{(z)}\right)\right] = 0.$$

We note that we can write this as

$$\frac{\partial h}{\partial t} - \nabla \cdot \mathbf{Q} = 0,$$

where $\mathbf{Q}(x,z,t)$ is the velocity flux. Physically this makes sense because divergence of the velocity field, for a fluid, gives the net rate of change of mass flowing from a point per unit volume. To get everything in terms of h we need to determine the relationship between p_x, p_z, and h. The normal stress balance gives that the change in momentum across the interface is balanced by the surface tension of the interface. Since the film is tangentially immobile at the surface, the quiescent nature of the fluid reduces the normal stress balance to

$$-p' = \gamma \bar{H},$$

but to leading order

$$\bar{H} \approx \nabla^2 h',$$

so we have

$$p = \frac{\gamma h_0^3}{\mu L^3 U_0}\left(\frac{\partial^2 h}{\partial x^2} + \frac{\partial^2 h}{\partial z^2}\right) = \sigma\left(\frac{\partial^2 h}{\partial x^2} + \frac{\partial^2 h}{\partial z^2}\right).$$

We note here that $\sigma = \epsilon^3/\text{Ca}$, where Ca is the capillary number. Substituting gives

$$h_t + \frac{\partial}{\partial x}\left(\frac{h^3}{3}[\sigma(h_{xxx} + h_{xzz}) + 1 + \lambda B F^{(x)}]\right)$$

$$+ \frac{\partial}{\partial z}\left(\frac{h^3}{3}[\sigma(h_{zxx} + h_{zzz}) + \lambda B F^{(z)}]\right) = 0. \quad (10)$$

We have thus obtained a fourth-order nonlinear differential equation for the free surface $h(x,z,t)$. We require a total of eight boundary conditions along with an initial condition to complete the formulation of the problem. We first assume that the film thickness is fixed at the boundary so that

$$h(0,z,t) = h(\alpha,z,t) = h(x,0,t) = h(x,\alpha,t) = h_b, \quad (11)$$

where h_b is the ratio of the half-thickness of the frame to the characteristic thickness of the film and α is the ratio of the frame size to the characteristic length scale. This is the same assumption that was made in Refs. [11,12]. For our problem $h_b \backsim 10^2$ and $\alpha \backsim 10$. We also require a no-flux condition through the boundary, which gives

$$Q_x = 0 \quad \text{at} \quad x = 0, \quad \alpha \quad Q_z = 0 \quad \text{at} \quad z = 0, \quad \alpha. \quad (12)$$

Given some initial profile $h(x,z,0) = f(x,z)$, we have completed the formulation of our mathematical model. We note here that, as expected, if we force h to have no z dependence, then our model reduces to the one formulated in Ref. [12]. In addition to boundary conditions (11) and (12), motivated by the experiments, we chose to consider a different set of boundary conditions consisting of the no-flux condition and a slope condition of the fluid at the boundary. That is,

$$h_x(0,z,t) = -\cot(\theta_c), \quad h_x(\alpha,z,t) = \cot(\theta_c),$$
$$h_z(x,0,t) = -\cot(\theta_c), \quad h_z(x,\alpha,t) = \cot(\theta_c), \quad (13)$$

where θ_c represents the contact angle at the fluid-frame interface. In the case where the frame thickness is much larger than the thickness of the film this seems to be a reasonable assumption to make. It is Eq. (10) with boundary conditions (11), (12), and (12), (13), which we explore for the remainder of the paper.

III. EXPERIMENTS AND NUMERICAL RESULTS

Now that the mathematical model has been developed, we wish to confirm that our model accurately describes the physical situation in question. In Ref. [12] it was shown that reverse drainage could be obtained with the presence of a magnetic field. Their model captures the essence of reverse drainage that is observed in experiments. The magnetic field was modeled as a large current loop with the film located at the center so as to have a magnetic field with only a vertical component. Here the gravitational force is competing with the force from the magnetic field. Once the magnitude of the magnetic force surpasses the gravitational force, reverse drainage occurs. This is clearly displayed in their results. With our mathematical model we note that the magnetic field will induce a force in both the vertical and horizontal directions. In validating the model, our approach will be to conduct experiments for multiple magnetic configurations and compare these results with results obtained from numerically solving
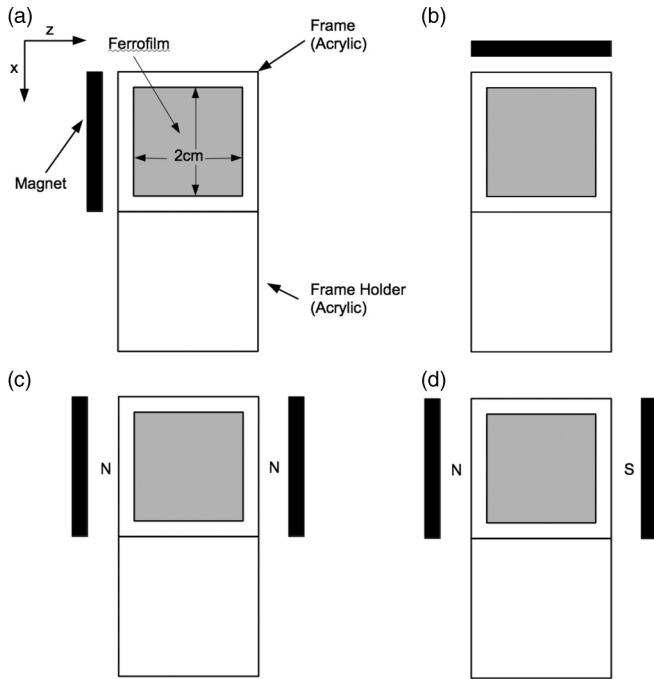
FIG. 2. Experimental setup for four different magnetic field configurations: (a) magnet on side, (b) magnet on top, and two magnets on side with (c) the same and (d) opposite polarity. The magnets have dimensions of $5 \times 5 \times 0.5$ cm^3.

the model. Once this has been done we can feel confident that this model will be valid for other magnetic configurations one might wish to consider.

A. Experiments

Our experimental setup consists of a ferrofilm suspended across an acrylic square frame (see Fig. 2). Similar to the experiments in Ref. [12], the ferrofilm solution consists of a soap solution and a nanoparticle ferrofluid solution. The nanoparticle solution is mixed in the following ratio: 4 ml of distilled water, 0.2 ml of commercial soap [14], 0.05 ml of gylercin and either 0.3 or 0.9 ml of ferrofluid. The ferrofluid consists of a uniform colloidal suspension of 10-nm iron oxide (Fe$_3$O$_4$) particles at 4% concentration [15]. We have subjected the film to a number of different magnetic fields. In each case neodymium magnets are used to generate the field. The field configurations (see Fig. 2) considered are the following: (i) a single magnet centered and placed on the left side of the frame, (ii) a single magnet above the frame, and two magnets place on both sides of the frame with (iii) the same (NN) and (iv) reverse (NS) polarity.

One part of the experimentation process we found to be challenging was the creation of a thin film that would be stable yet drain to a significant amount of black film. We found that adding just the right amount of glycerine is crucial. When too little glycerine was added the film ruptured quickly and we could not get good results. When too much glycerine was added the film drained a while, but then became static before any significant formation of black film occurred. There seemed to be a delicate balance, which allowed the film to sustain but still form a large black film region. Another

thing we observed was the difference between dipping the frame in solution to form the film and blowing a bubble onto the frame to form the film. When the frame was dipped we observed an excess amount of fluid in the film, which resulted in a significant amount of convection. This higher-order effect definitely changed the overall behavior of the film in comparison to the leading-order model we constructed. Blowing the bubble resulted in a film with less fluid and as a result the convection was greatly reduced. Although there were still some pockets in the film where convection was present, it did not appear to affect the overall behavior of the film. After testing multiple solutions we found one that worked quite well. Our films were stable enough to drain the bulk of the fluid in approximately 60 s. After this we observed steady growth of the black film region until rupture.

In observing the films we looked at two different aspects of the drainage. The first is the drainage of the bulk of the fluid, which occurred over a time scale of approximately 60 s. From the moment the fluid was in the presence of the magnetic field the drainage and structure was affected. The structure of the bulk remained throughout the drainage process. The second is drainage of the regions of black film and white film that appear shortly after the film is created. The black film is a thin region with a thickness of approximately 10 nm. The white film region has a thickness less than 100 nm [3]. We observed that the white region seemed to be affected more by the magnetic field and the black film was not affected at all by the magnetic field. In the black film region there should be no iron oxide particles since the size of the particles is larger than the thickness of the film. As for the white region, it is not clear why the difference has occurred. It could be that as the film thins more ferroparticles get trapped in this region, creating a higher concentration of particles, as suggested in Ref. [10]. This might explain the difference in behavior between the white film and the bulk of the fluid in the film.

The experiments were carried out as follows. We created an acrylic frame with slots on each side to hold the neodymium magnets with a separate frame cutout that can be removed from the middle. Once the magnets were set in the desired configuration a bubble was blown to create a soap film across the frame. We then let the film drain until rupture. We were interested not only in the structure based on the magnetic field but also in how we could control the effect. Since our magnets used are permanent, directly varying the field strength was not an option. We chose to consider varying the distance from the magnet to the film, which was done in Ref. [12], and varying the amount of ferrofluid in the film solution. Varying the amount of ferrofluid will change the magnetic susceptibility of the film and thus its behavior in the presence of the magnetic field. We had two film solutions with different amounts, 0.3 and 0.9 ml, of ferrofluid giving magnetic susceptibilities of 0.01 and 0.03, respectively. For each configuration, multiple trials were run and consistent results were obtained. The experimental images are shown at times of 0, 20, 40, and 60 s.

For configuration (i) a magnet is placed to the left of the film. In all cases the film would drain to mostly black and white film in approximately 60 s. The film would have a slope as it drained. The slope in all cases was more pronounced for the white film than for the bulk of the fluid (see Fig. 3). In particular (see Ref. [16]), when the magnet is 30 mm from the
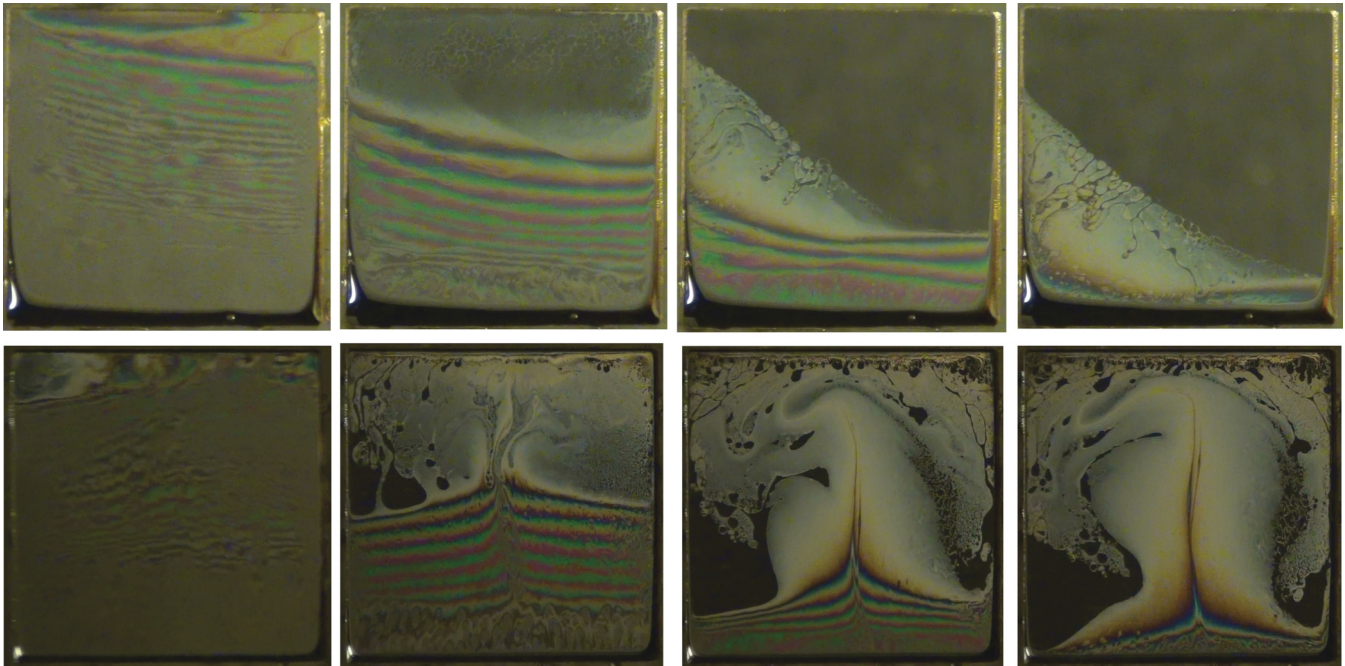
FIG. 3. (Color online) Experimental pictures at times of 0, 20, 40, and 60 s progressing from left to right. The pictures on top and bottom correspond to configurations (i) and (ii), respectively, as shown in Fig. 2, where the magnets are 20 mm away from the film and χ_m is 0.03. Notice the central channel and the sharp V shape in configuration (ii). For configuration (i) the interaction between gravity and the magnet pulls the fluid to the lower left-hand corner. Increasing the distance or decreasing χ_m will decrease the slope (see Ref. [16]).

film the fluid as it drains has no apparent slope, but the white film has a large slope. The slope of the fluid increases with decreasing distance and/or increasing χ_m.

For configuration (ii) (see the bottom row of Fig. 3) the amount of reverse drainage depended on the strength of the magnet and distance to the film. When the magnet was placed 30 mm away the film would drain under gravity and the magnet had very little effect on the film. However, the films still drained slower than drainage under gravity [16]. The slowing down of drainage by a magnetic field was observed in Ref. [10]. The film with the higher magnetic susceptibility had slightly more white film. When the magnet was moved closer the images show clear reverse drainage [16]. Also note that in all cases where reverse drainage is present the fluid is moving up through a central channel. We noticed that increasing the field strength and/or decreasing the distance from the magnet to the film would change where the region of black film would form. For a strong magnet ($B = 1.5$ T at 5 cm from the magnet) placed 10 mm from the frame edge we have complete reverse drainage and the black film forms at the bottom of the film (see the bottom row of Fig. 4). We also considered an asymmetric case where the magnet on top was offset from the film. In the top row of Fig. 4 the magnet is above the film as before but shifted to the right such that the left edge of the magnet is located directly above the center of the film. Notice that the fluid collects in the upper and lower right-hand corners of the frame.

For configuration (iii) a magnet is placed on the left and the right of the film with the north poles of the magnets facing each other (NN) [see the diagram in Fig. 2(c)]. The film forms a V shape (see the top row of Fig. 5). Also note that the white film has a much more pronounced V shape than the bulk of the fluid. However, the V shape for the bulk of the fluid does increase

with decreasing distance to the magnet and increasing χ_m (compare the top row of Fig. 5 to Ref. [16]). We also considered an asymmetric case where the magnet on the left is 20 mm away from the film and the magnet on the right is 30 mm away. This results in a shift of the V shape so that the tip of the V is still at the centerline between the magnets. For configuration (iv) a magnet is placed on the left and the right of the film and the magnets are attracted to each other (NS) [see the diagram in Fig. 2(d)]. Experimentally we see that the fluid does not have a sharp V shape like the NN case. When the magnets are offset and the magnet on the right is moved to a distance of 30 mm, the fluid drainage resembles the case for configuration (i).

In all cases it is clear that the film is affected by the presence of the magnetic field and clearly adheres to the structure of the field. In all cases the field has a stronger influence on the white film region than on the bulk of the fluid. Both varying the distance of the magnet to the film and varying the ferrofluid concentration change the effect on the film. In Ref. [16] we have the experimental results for the main configurations with the low ferrofluid solutions as well as for varying distances.

B. Numerical investigation

In this section we perform a numerical investigation of the mathematical model and compare with the experimental results. Due to the nature of the model developed in Ref. [12], replacing the permanent magnet in the experiment by a circular loop in the model is a valid approximation to make. Since we would like to see how the added dimension aids in describing the structure of the entire film, this model will not work for us. To model our permanent magnet we consider it to be a collection of magnetic dipoles. This lends itself well to
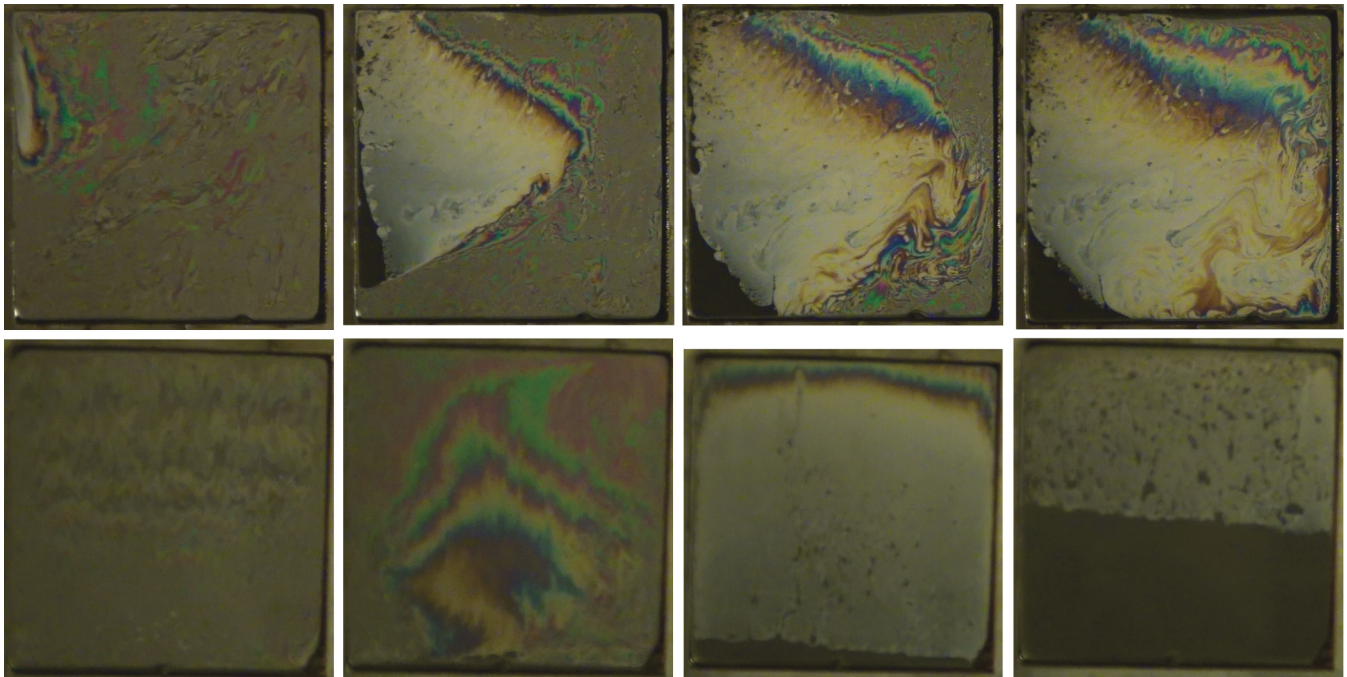
FIG. 4. (Color online) Experimental pictures at times of 0, 20, 40, and 60 s progressing from left to right. The top row is configuration (ii) with the magnet offset to the right. The bottom row is for a strong magnet ($B = 1.5$ T at a distance of 5 cm from the magnet) in configuration (ii). The strong magnet gives complete reverse drainage with the black film region forming on the bottom first and the fluid drains up.

numerical computations. We simply replace each permanent magnet by a rectangular lattice with dipoles at the vertices (Fig. 6). The field strength of our magnets are measured to be $B = 0.095$ T at a distance of 5 cm from the center of the magnet. This is used to normalize the magnetic field in the code. For our numerical calculations we used a lattice of $50 \times 50 \times 5$ dipoles to model the magnet, which has dimensions of $5 \times 5 \times 0.5$ cm^3. Increasing the number of dipoles further had no noticeable effect on the model. In the Appendix we have included plots of the magnetic field lines and the
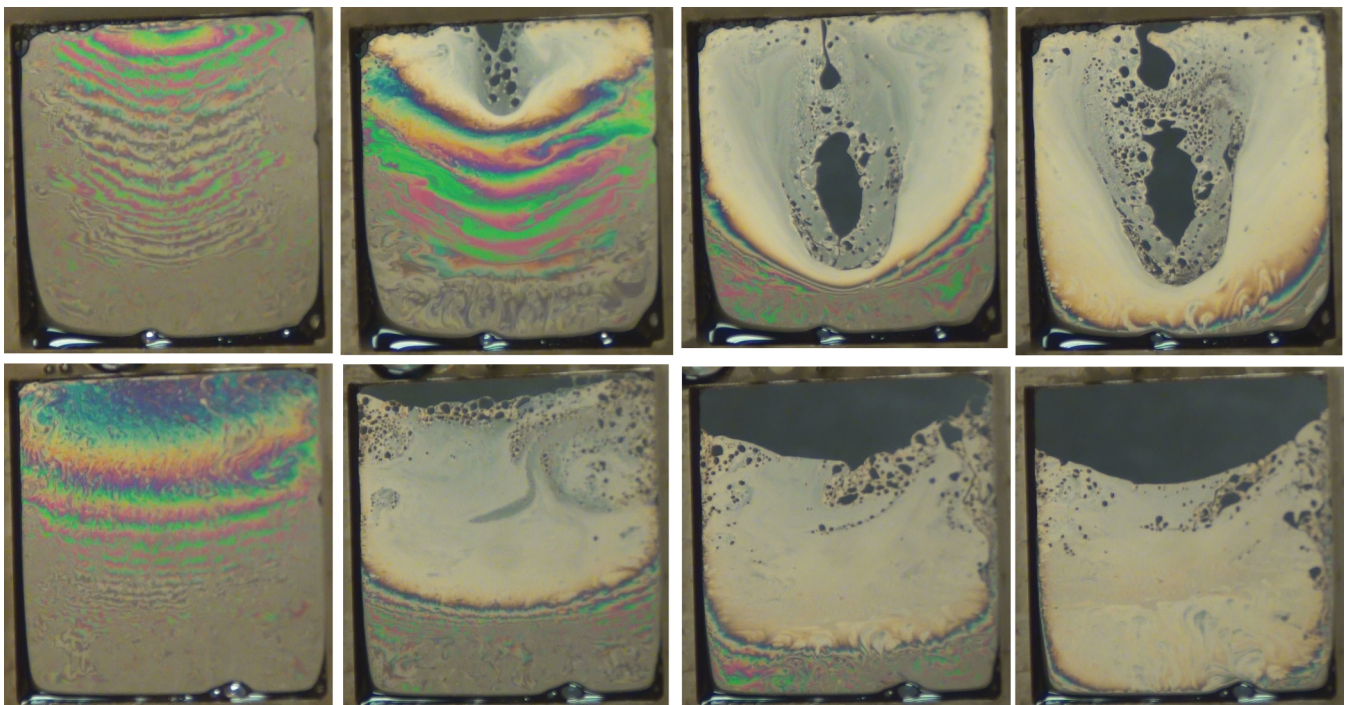

FIG. 5. (Color online) Experimental pictures at times of 0, 20, 40, and 60 s progressing from left to right. The pictures on top (bottom) correspond to the NN (NS) configuration shown in Fig. 2, where the magnets are 20 mm away from the film and χ_m is 0.03. Notice the pronounced V shape for the NN configuration.

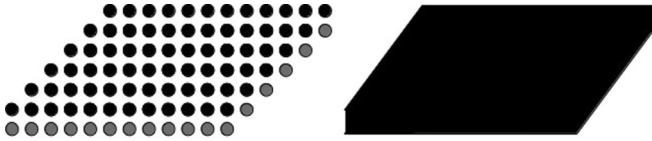FIG. 6. For the numerical calculations we model the magnet, which has dimensions of $5 \times 5 \times 0.5$ cm^3, as a lattice of $50 \times 50 \times 5$ dipoles. Increasing the number of dipoles further had no noticeable effect on the model.

body force (BF) for each of the magnet configurations in our experiments.

A second-order finite-difference approach is used to discretize the differential equation. Since our boundary conditions involve the components of the flux vector, we consider solving the problem at the halfway points. This approach was used in Ref. [11] for the one-dimensional (1D) model discussed above. Once we discretize the problem in space we obtain a system of equations for the time derivative at the grid points. From here we use the method of lines to solve the problem forward in time and observe the evolution of the film. In this section we wish to display the results of the numerical simulations and discuss their ability to capture the behavior of the experiments. Table I gives a list of the physical parameter values used for the numerical simulations. We point out that the susceptibility constant χ_m is based on the concentration of magnetite in our thin film solution. Since we ran experiments with two different ferrofluid concentrations, we have two corresponding χ_m values.

The model does a good job of predicting the behavior of the bulk of the fluid. However, the model does not seem to account for the dominant effect the magnetic BF has on the white film regions seen in the experiments. In Sec. III A we described four different magnetic configurations. We explore these setups numerically by changing the locations of our dipoles to match the desired configuration. In our numerical simulations we considered changes in χ_m, changes in the distance of the magnets to the film, and changes in the boundary conditions of the film. For all situations we considered a flat initial profile. For boundary condition (11) we set the initial thickness to the thickness of the frame. For boundary condition (13) we set the initial thickness to be h_0. In this section we show the results for boundary condition (13) with $\chi_m = 0.03$ and the closer distance of 20 mm from magnet to frame. Although we will discuss the situation of boundary condition (11), we have placed the figures for these simulations in Ref. [16]. The contact angle of the film to the frame was difficult to determine. In our simulations we use a representative angle

TABLE I. List of the parameters used in our model.

Parameter	Value
g, acceleration of gravity	9.8 m/s^2
ρ, density of solution	1100 kg/m^3
γ, surface tension	0.042 N/m
μ, viscosity	2 cP
μ_0, magnetic permeability	$4\pi\,10^{-7}$ N/A^2
B_0, magnetic field	0.095 T
χ_m, magnetic susceptibility	0.01 and 0.03

of $\pi/4$. We ran simulations for all of the scenarios considered in the experiments and found the change in behavior due to varying the amount of ferrofluid in the solution and varying the distances was consistent with experimental results. That is, reducing the ferrofluid concentration and/or increasing the distance showed a reduction in the magnets effect on the film. For this reason we give the result for the case of larger ferrofluid concentration and closer distance.

We begin with configuration (i) where the magnet is to the left of the frame. The magnetic and the BF field lines are given in the Appendix, see Figs. 12 and 13. Figure 7 shows a series of images at $t = 0, 20, 40$, and 60 s as the fluid drains from its initial flat profile. The model shows a slope for the draining fluid as seen in the experiments. The model correctly predicts that the slope will increase with increasing χ_m and decreasing distance. Although there is some evidence of the angled structure of the thin region as it drains, it is not as noticeable in the simulations as in the experiments. Notice that the bulk of the fluid builds up in the lower left corner of the frame in the model and grows out from there. The changes in ferrofluid concentration and magnet distance reduced the slope of the draining fluid in the simulation, which agrees with our experimental observations. When boundary condition (12) was introduced the main effect was to push the bulge away from the lower left-hand corner. The fluid is pushed away from the corner to satisfy the fixed boundary condition. As to whether this is a better description of the experiment or not is difficult to determine. We definitely see a large collection of fluid in the bottom corner. It is hard to tell whether or not all of the fluid has pushed into one region. Overall, the qualitative behavior of the bulk of the fluid collecting in the lower corner is captured by both models.

For configuration (ii) we have a magnet on top (Fig. 8). The magnetic and the BF field lines for configuration (ii) are given in the Appendix, see Figs. 12 and 13. For a case where the magnet is on top and centered above the frame the simulation agrees well with experiment. At a distance of 30 mm where there is no apparent reverse drainage the magnet still slows down the drainage of the film, which is in agreement with our experiments and Ref. [10]. Also note that in the model there is a channel of increased thickness going up the middle of the film, which agrees with the experiments, showing that for the case of reverse drainage there is a channel of fluid moving up through the middle of the film. The model also shows a slight bulge at the top and bottom of the frame for partial reverse drainage. In the experiments the bulk fluid has more of a sharp peak (Fig. 3). Similar to configuration (i), reducing the ferrofluid and increasing the distance reduce the effect of the magnet on the film. When simulations were done for the lower concentration and farther distance there was no appearance of reverse drainage, but drainage was slowed compared to drainage under gravity [16]. When the magnet is moved closer and/or a stronger magnet is used the region where the black film is formed moves further down the film, which agrees with our experiments and Ref. [12]. In particular, when we use a strong magnet ($B = 1.5$ T) and place it 10 mm from the top of the frame we get complete reverse drainage in both the model and experiments. In the case where the magnet is above the frame and offset to the right we see that the simulation agrees well with the experiments, showing that the fluid is pulled to the upper and
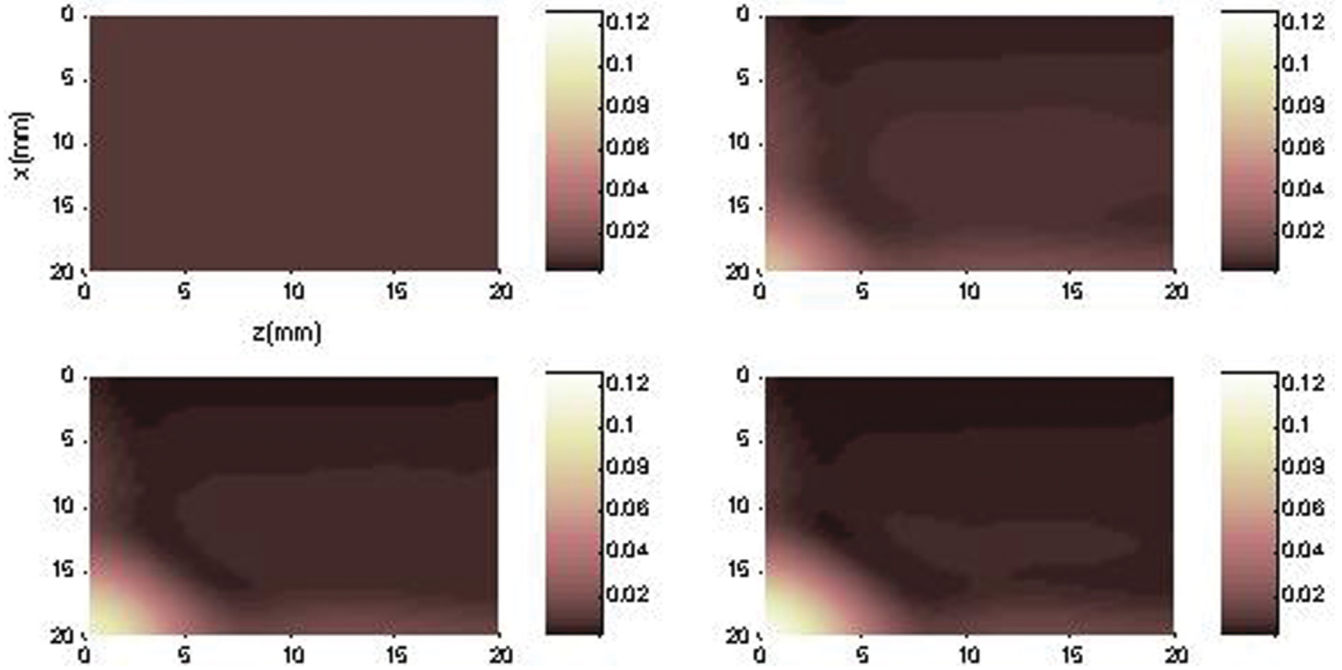
FIG. 7. (Color online) Simulations for configuration (i) with $\chi_m = 0.03$ and the magnet 20 mm from the film. The frames shown are for times $t = 0$, 20, 40, and 60 s. The times progress left to right with $t = 0$ in the top left corner. The fluid collects in the lower left corner as time progresses. The thin region grows, which is in agreement with experiment (see Fig. 3).

lower right corners of the frame (compare Fig. 4 to Fig. 9). For boundary condition (12) the peaks in the center are more pronounced, which is in better agreement with experiment.

For configuration (iii) we have a magnet on the left and right of the film with the north poles facing each other (NN).

The magnetic and the BF field lines for configuration (iii) are given in the Appendix, see Figs. 12 and 13. The model correctly predicts that the bulk of the fluid is drawn to the lower left and right corners of the frame. However, it does not predict the pronounced V shape seen in the white film in the experiments.
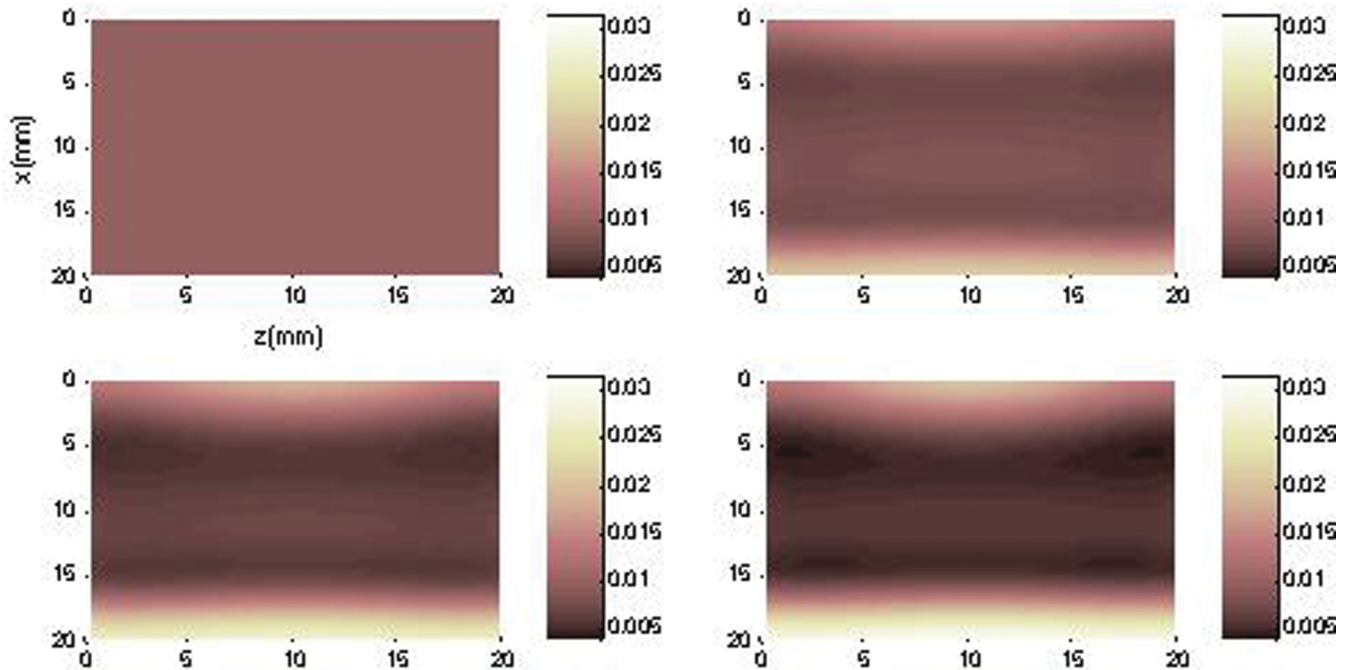

FIG. 8. (Color online) Simulations for configuration (ii) with $\chi_m = 0.03$ and the magnet 20 mm from the film. The frames shown are for times $t = 0$, 20, 40, and 60 s. The times progress left to right with $t = 0$ in the top left corner. The film undergoes partial reverse drainage. However, the model does not give the sharp peak as seen in the experiment.
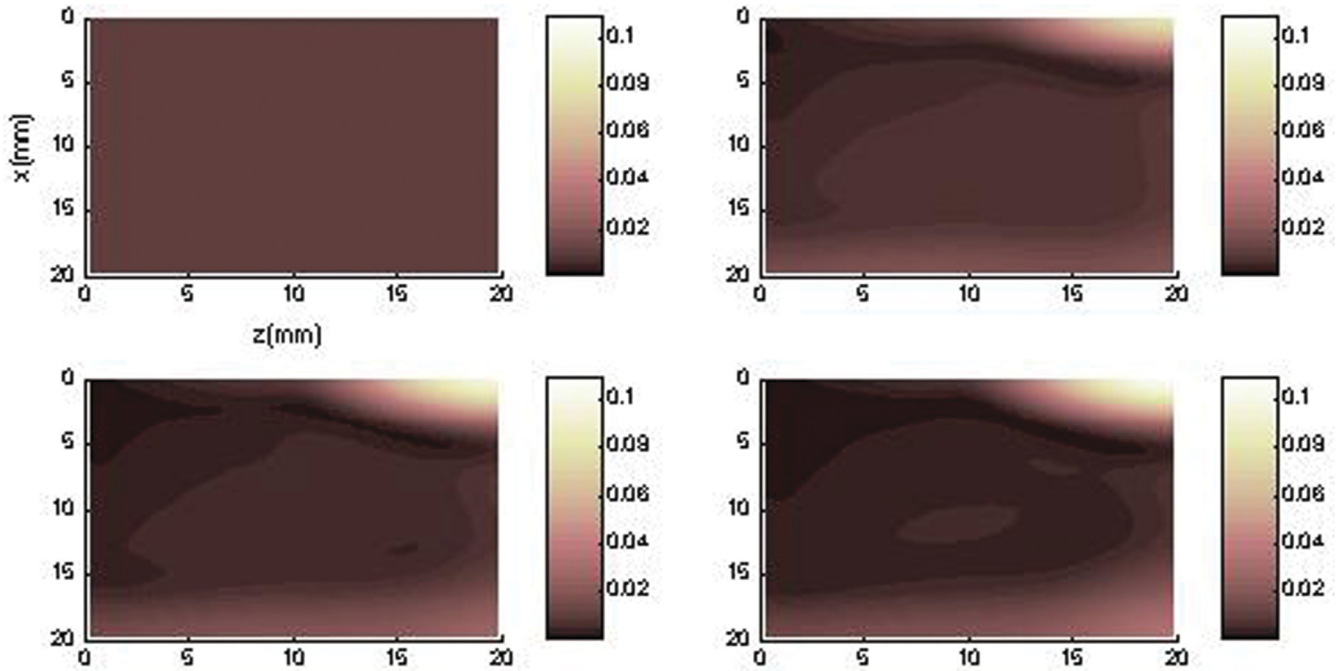
FIG. 9. (Color online) Simulations for configuration (ii) with the magnet offset to the right. The frames shown are for times $t = 0, 20, 40,$ and 60 s. The times progress left to right with $t = 0$ in the top left corner. The simulation is for a magnet 10 mm from the top of the film. We use a closer distance to magnify the effect of the magnet on the film. The simulation is in good agreement with experiment (see Fig. 4).

We feel this might be due to dipole-dipole interactions within the film. For the NN configuration the dipoles near the center of the film will repel each other, a facet that our model does not capture. When boundary condition (12) is used the separation is less pronounced. Boundary condition (13) seems to agree better with the experiments. After 60 s the majority of the film is less than 100 nm in thickness and there is very little fluid collected at the bottom in the center.

For configuration (iv) we have a magnet on the left and right of the film with the magnets attracted to each other (NS).
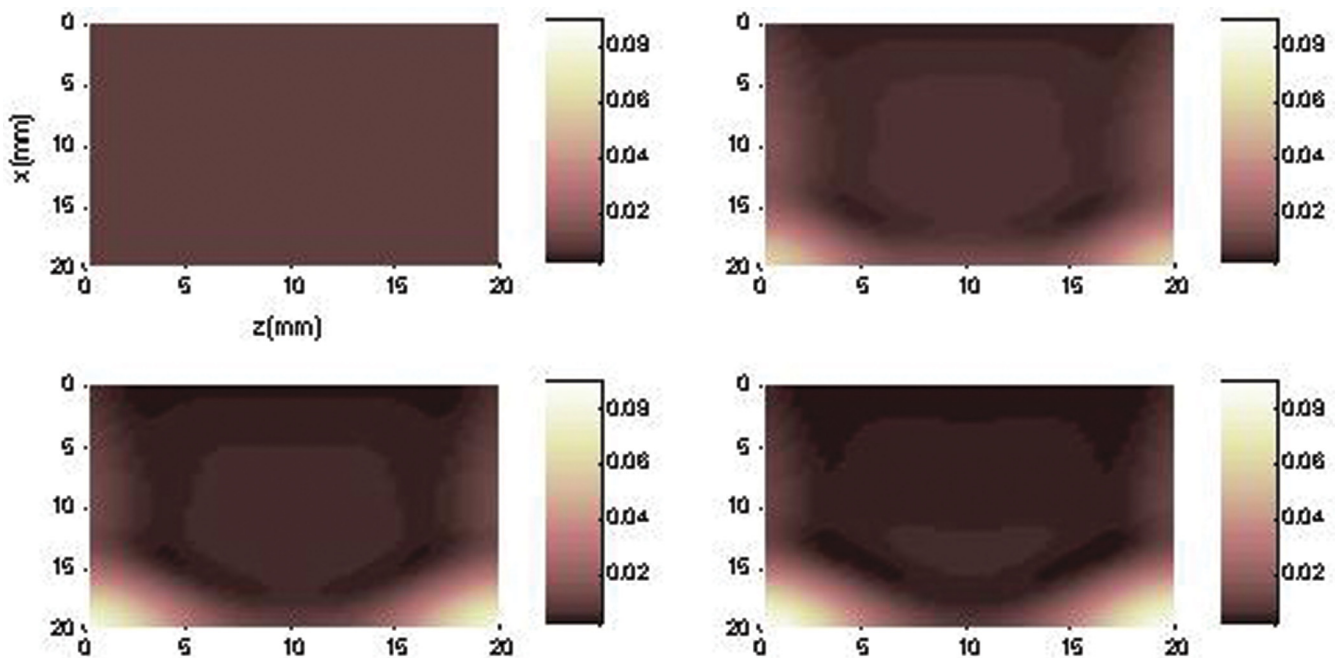

FIG. 10. (Color online) Simulations for configuration (iii) with $\chi_m = 0.03$ and the magnets 20 mm from the film. The frames shown are for times $t = 0, 20, 40,$ and 60 s. The times progress left to right with $t = 0$ in the top left corner. The simulation shows the fluid draining to the lower left and right corners of the frame, in agreement with experiment (see Fig. 5). However, the model does not predict the pronounced V shape seen in the experiment.

The Appendix gives the field lines and BF for configuration (iv), see Figs. 12 and 13. The model correctly predicts that the bulk of the fluid is drawn to the lower left and right corners of the frame. The fluid in the model appears to have a more pronounced V shape for the NS configuration than the NN configuration, which does not agree with experiment. However, in the experiment we can see the 2D structure of the film by looking at the thinnest parts of the film, not where the fluid bulges out in the lower corners of the frame. Looking at the thinnest parts of the film in Figs. 10 and 11, we see there is not much difference between the NN and NS configurations. Comparing the body forces in the Appendix, we see that they differ in the center of the frame where it is the smallest and gravity would dominate in that region of the film. Overall we feel that the model does a good job of capturing the bulk behavior of the fluid. Boundary condition (12) has an effect similar to that of the NN configuration. That is, the separation of the peaks is less pronounced.

We would like to comment on the differences seen in the simulations for the NN and NS configurations and the experiments. We believe the differences could be due to dipole-dipole interactions within the fluid (see Ref. [10]), which our model does not account for. In particular, Ref. [10] noted that this dipole-dipole force would be present for all external fields and generate macroscopic effects. When the fluid is in the presence of an external magnetic field the iron particles line up with the field and a force is induced on the fluid. When this occurs the fluid is magnetized, based on the alignment of the magnetite particles. Based on the alignment structure, these particles, and thus the fluid, will either attract or repel each other. For example, for the NN configuration the particles on the left side of the film will align in such a way

that they should repel the particles on the right side of the film. This in turn should give an added push of the left portion of the film to the left magnet and right portion to the right magnet. This would account for the clear separation seen in the white film and black film region as well as the pronounced V shape of the bulk as it drains. In contrast, for the NS configuration the particles on the right and left should align in such a way that they, and thus with film, will be attractive. This would have a smoothing effect and the V-shape structure would be less pronounced. We also feel that this interaction enhances the peak at the bottom for the magnet on top configuration.

IV. DISCUSSION

In Ref. [12] a 1D model was developed that showed reverse drainage. We wanted to extend those results to two-dimensions and see if we could reproduce the structure seen in experiment. The model shows good agreement with the bulk of the fluid for many different magnetic field configurations. The model showed good agreement with experiment as we varied the distance and positions of the magnet (or magnets) and the concentration of the ferrofluid in the solution. We feel that these results show that the model is robust. However, the model did not have good agreement with the white film region. Our experiments show that the white film region is more strongly affected by a magnetic film than the bulk of the fluid. The authors of Ref. [10] noticed this behavior as well. Another difference between the model and experiment is the dipole-dipole interactions within the film [10]. Dipole-dipole interactions within the film are not accounted for in our model. This might explain the difference between the model and experiment for the NN and NS configurations. According to the model, the NN and NS configurations should look very similar.
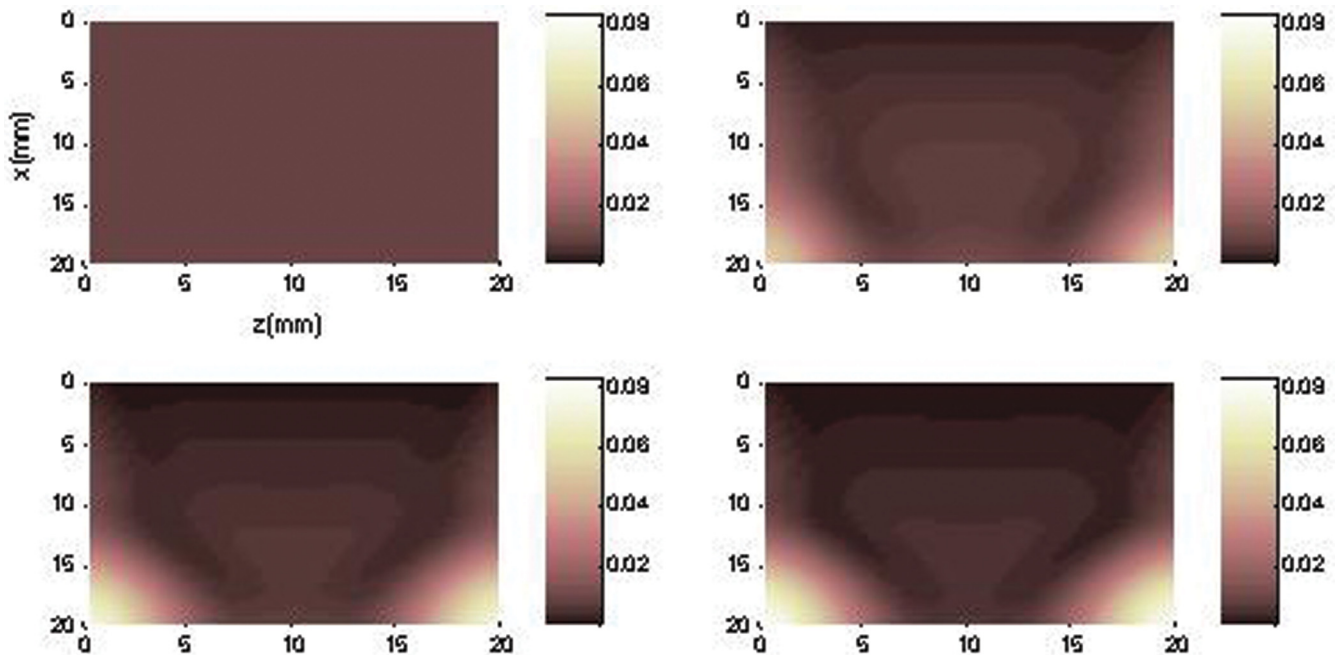

FIG. 11. (Color online) Simulations for configuration (iv) with $\chi_m = 0.03$ and the magnets 20 mm from the film. The frames shown are for times $t = 0, 20, 40,$ and 60 s. The times progress left to right with $t = 0$ in the top left corner. The simulation shows the fluid draining to the lower left and right corners of the frame, in agreement with experiment (see Fig. 5).

However, in the experiment there is a noticeable difference between the NN and NS configurations in the white film region. The experiments for the NN and NS configurations are similar in the bulk of the fluid, but not in the white film region. For the top configuration the experiments show a sharper peak in the middle regions than the model shows; this could also be due to dipole-dipole interactions. We feel that overall the model agrees well with experiment. By extending to two dimensions and looking at a variety of magnetic field configurations we feel that the range of physical systems that this model could be used to describe has been greatly enhanced.

Two models were used and compared to experiment. One model had a fixed boundary and one had a moving boundary with a slope condition. Both models showed good agreement with experiment for the bulk of the fluid. The fixed boundary gave good agreement when the initial profile was flat and initial thickness was equal to the thickness of the frame. In our experiments the frame had a thickness

of $\sim$2 mm, which is orders of magnitude larger than the thickness of a typical soap film. The moving boundary model could be given a more realistic initial profile and show good agreement with experiment. The moving boundary model is a better description of our physical experiment. However, from a modeling standpoint, both boundary conditions are important and represent possible physical systems involving ferrofilms.

One aspect of the physical system, which we have not mentioned until now, is the possibility of a steady state configuration for the draining soap film. It was observed in Refs. [11,12] that the drainage of the film slows with time and approaches a steady state, although they did not observe this experimentally. In Ref. [11] an analysis of the steady state solutions for the 1D model based on the numerical simulations approaching a steady state was performed. We observed a similar behavior for our numerical simulations. That is, as time progressed the solution reached a point where there was little to no observable change in the profile. Although our
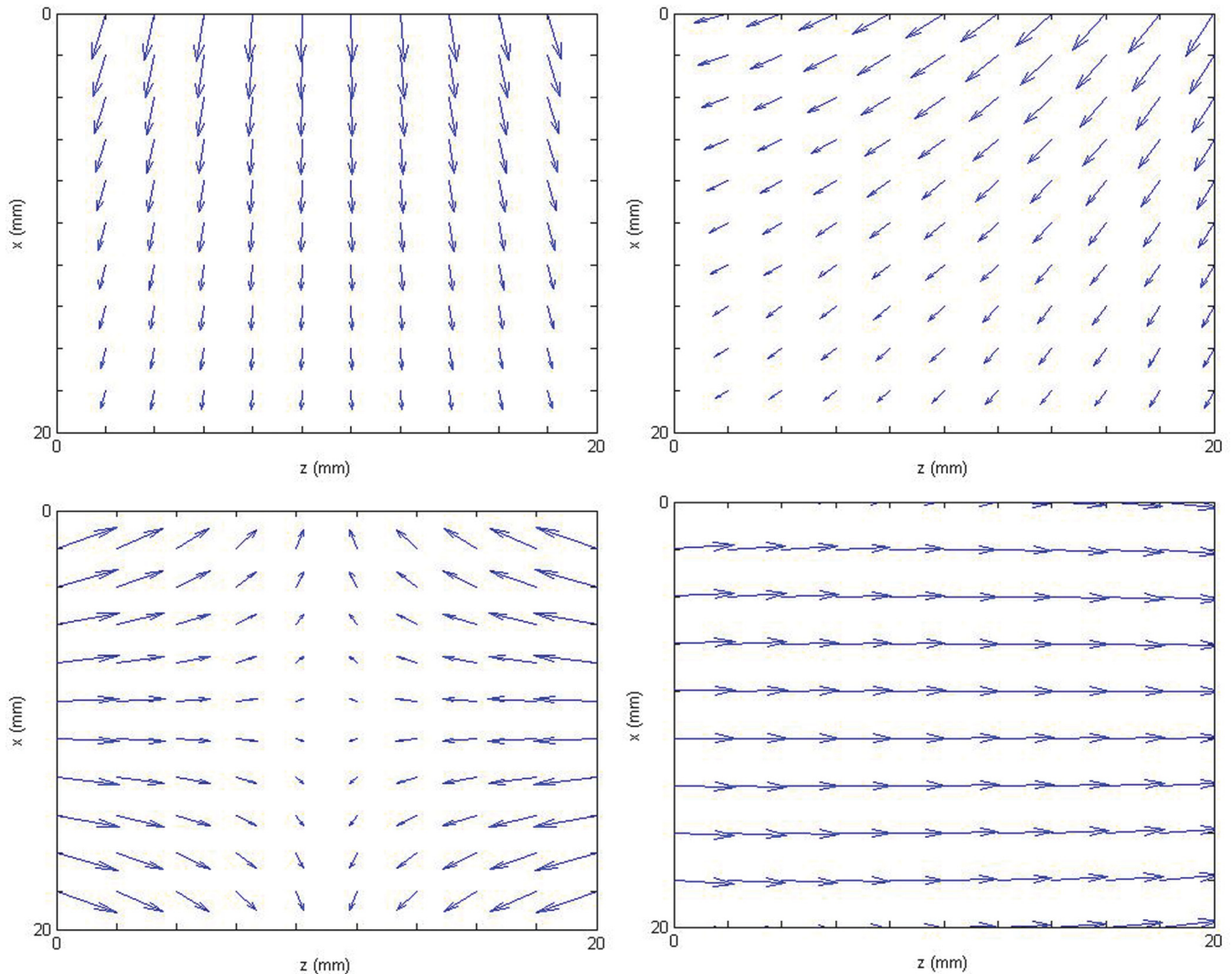

FIG. 12. (Color online) Magnetic field for different magnet configurations. The top left figure is for configuration (ii) and the top right figure is for configuration (ii) but with the magnet offset to the right. The bottom left figure is for configuration (iii) and the bottom right figure is for configuration (iv). For configuration (i) the top left image can be rotated by 90°.

model and the one in Ref. [11] are both nonlinear, the added dependence on the *z* component removed the ability to perform an initial integration of the steady state equation, as was done in Ref. [11], which allows one to deal with the problematic nonlinearity. As for the experiments, it was observed that the bulk of the drainage occurred over a rather sort time span; however, the film ruptured before an observable steady state was reached. The steady state structure of this system is definitely a topic of interest and we leave this as an area for future research.

One obvious challenge we faced was the creation of a good ferrofilm solution. We were able to create films with a significant amount of black film before rupture. We also found that blowing the film onto the frame reduced the amount of convection in the film. This is important because we developed a leading-order model that does not capture higher-order effects such as convection. By blowing the film onto the frame we create a much thinner film than you would have by dipping the frame. In the experiments we

were restricted to using neodymium magnets because of the large field needed to manipulate the fluid in the film. On a microscale or nanoscale it may be possible to use current-carrying loops to generate the magnetic field. This would allow more control over the structure and strength of the field, which in turn would allow for more control over the structure of the film. In carrying out the experiments for this paper we also created rectangular films (vertical sides being shortest), circular films, and cylindrical films. The cylindrical film was by far the most interesting, but it would require a complete reworking of the model. This is a topic left for future exploration.

APPENDIX

In this Appendix the magnetic field and body force are given for different magnet configurations in Figs. 12 and 13, respectively.
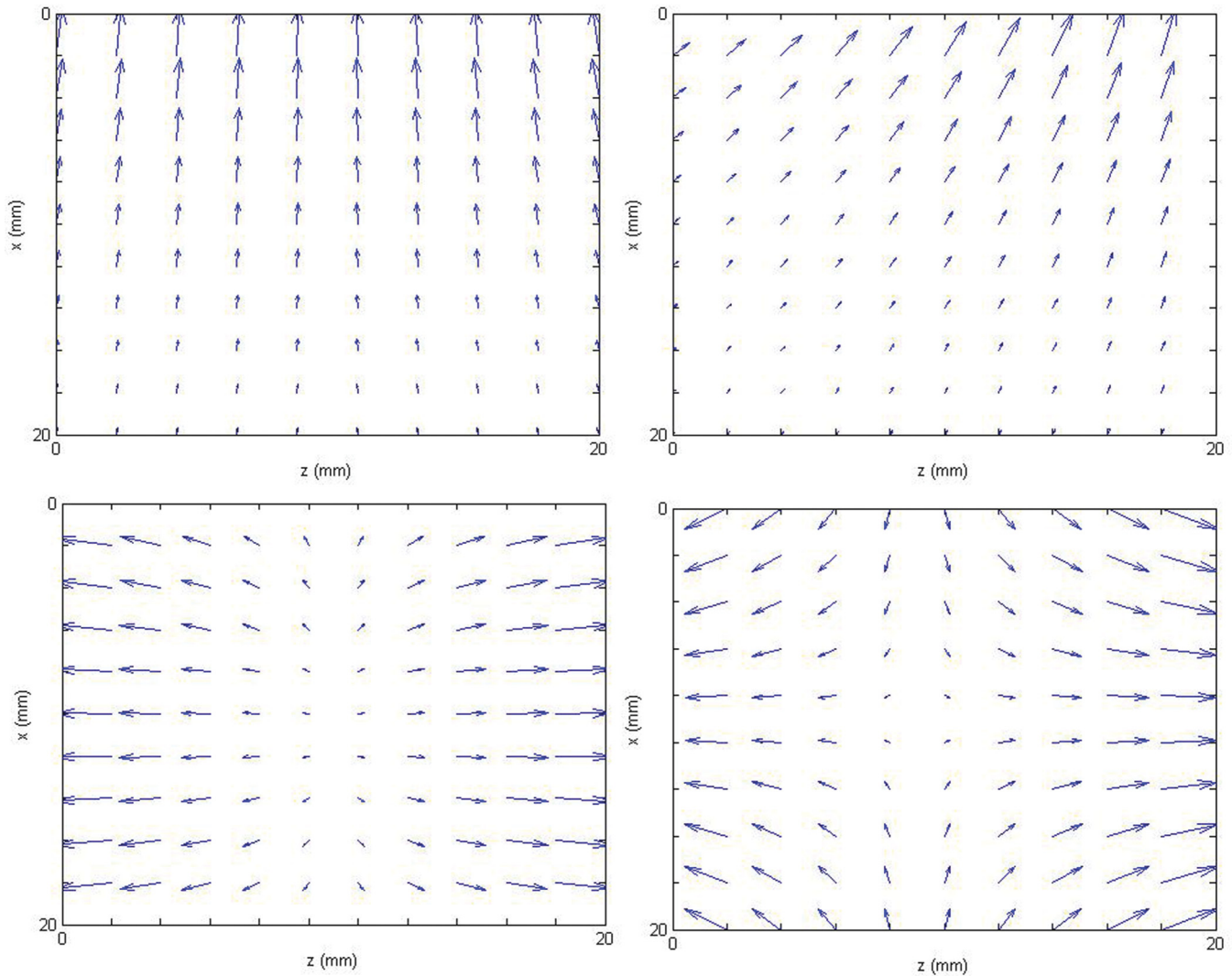

FIG. 13. (Color online) Body force for different magnetic configurations. The top left figure is for configuration (ii) and the top right figure is for configuration (ii) but with the magnet offset to the right. The bottom left figure is for configuration (iii) and the bottom right figure is for configuration (iv). For configuration (i) the top left image can be rotated by 90°.

[1] K. J. Mysels, K. Shinoda, and S. Frankel, *Soap Films, Studies of their Thinning and a Bibliography* (Pergamon, London, 1959).

[2] P. Grinfeld, Phys. Rev. Lett. **105**, 137802 (2010).

[3] C. Isenberg, *The Science of Soap Films and Soap Bubbles* (Tieto Ltd., Clevedon, England, 1978).

[4] M. D. Cowley and R. E. Rosenswe, J. Fluid Mech. **30**, 67 (1967).

[5] R. E. Rosensweig, *Ferrohydrodynamics* (Cambridge University Press, New York, 1985).

[6] R. M. Oliviera, J. A. Miranda, and E. S. G. Leandro, Phys. Rev. E **77**, 016304 (2008).

[7] H. D. Liu, W. Xu, S. G. Wang, and Z. J. Ke, Appl. Math Mech. **29**, 1341 (2008).

[8] S. S. Nair, S. Rajesh, V. S. Abraham, and M. R. Anantharaman, Bull. Mater. Sci. **34**, 245 (2011).

[9] N. T. Nguyen, Microfluidic. Nanofluidic. **12**, 1 (2012).

[10] F. Elias, J.-C. Bacri, C. Flament, E. Janiaud, D. Talbot, W. Drenckhan, S. Hutzler, and D. Weaire, Colloids Surf. A **263**, 65 (2005).

[11] D. E. Moulton and J. Lega, Physica D **238**, 2153 (2009).

[12] D. E. Moulton and J. A. Pelesko, Phys. Rev. E **81**, 046320 (2010).

[13] D. J. Griffiths, *Introduction to Electrodynamics*, 3rd ed. (Prentice Hall, Englewood Cliffs, NJ, 1999).

[14] Dawn^TM was used.

[15] Solution EMG 705 obtained from Ferrotec Corporation.

[16] See Supplemental Material at http://link.aps.org/supplemental/10.1103/PhysRevE.86.046301 for more experimental results involving different ferrofluid concentrations and magnetic configurations as well as numerical simulations for both sets of boundary conditions.